PTEP

Prog. Theor. Exp. Phys. **2016**, 083I01 (23 pages)
DOI: 10.1093/ptep/ptw094

Theory of time-reversal topological superconductivity in double Rashba wires: symmetries of Cooper pairs and Andreev bound states

Hiromi Ebisu[1,*], Bo Lu[1], Jelena Klinovaja[2], and Yukio Tanaka[1]

[1]*Department of Applied Physics, Nagoya University, Nagoya 464-8603, Japan*
[2]*Department of Physics, University of Basel, Klingelbergstrasse 82, CH-4056 Basel, Switzerland*
[*]E-mail: ebisu@rover.nuap.nagoya-u.ac.jp

Received March 8, 2016; Revised May 23, 2016; Accepted June 1, 2016; Published August 2, 2016

We study the system of double Rashba wires brought into proximity to an *s*-wave superconductor. Time-reversal invariant topological superconductivity is realized if the interwire pairing, corresponding to a crossed Andreev reflection, dominates over the standard intrawire pairing. We classify the symmetry of the Cooper pairs focusing on four degrees of freedom, i.e., frequency, spin, spatial parity inside wires, and spatial parity between wires. The presence of the spatial parity between wires is a unique feature of this model. The magnitude of the odd-frequency pairing is strongly enhanced in the topological state irrespective of spatial parities. We also explore the properties of junctions occurring in such double-wire systems. If one section of the junction is in a topological state and the other is in a trivial state, the energy dispersion of the Andreev bound states is proportional to $\sim \pm \sin\varphi$, where φ denotes the macroscopic phase difference between the two sections. This behavior can be intuitively explained by the couplings of a Kramers pair of Majorana fermions and a spin-singlet *s*-wave Cooper pair and can also be understood by analyzing an effective continuum model of the $s + p$/*s*-wave superconductor hybrid system.

Subject Index I60, I63, I68

1. Introduction

The concept of topology [1,2] and topological effects has attracted a lot of attention over recent decades. For example, the appearance of the zero-energy surface Andreev bound state (SABS) in unconventional superconductors like *p*-wave [3,4] or *d*-wave superconductors [5–7] has been understood in terms of the topological invariants defined for the bulk Hamiltonian [8–11]. Also, the possibility of generating an effective topological *p*-wave superconductivity in systems coupled to conventional *s*-wave superconductors due to internal spin structure [12–24] opened the field for experiments [25–30]. In 1D systems, zero-energy SABSs are Majorana fermions (MFs), which are of great importance for topological quantum computing [31,32].

In this context, it is useful to shed light on MF physics from different angles. One aspect not covered in the literature on MFs is the symmetry of Cooper pairs in the topological regime. Generally, if we consider such a degree of freedom as time as well as space and spin, there are four possible symmetries of Cooper pairs: even-frequency spin-singlet even-parity (ESE), even-frequency spin-triplet odd-parity (ETO), odd-frequency spin-triplet even-parity (OTE) [33], and odd-frequency spin-singlet odd-parity (OSO) [34–36]. It is known that the odd-frequency pairing exists ubiquitously in inhomogeneous superconductors [9,37], and it is hugely enhanced at the boundaries if zero-energy

SABSs are present [9,37–40]. The connection between MFs and the odd-frequency pairing has also been clarified before now in several systems [24,41–43]. It was shown that MFs inevitably accompany odd-frequency spin-triplet pairing in D-class topological superconductors with broken time-reversal symmetry [41].

Alternatively, there are also time-reversal invariant topological superconductors belonging to the topological DIII class [1,2] and occurring in various condensed-matter systems [44–47]. If the time-reversal symmetry is not broken, two MFs come in Kramers pairs and are protected from splitting [48–62]. In this work, we focus on a system consisting of two quantum wires with Rashba-type spin–orbit interaction (SOI) brought into proximity to an *s*-wave superconductor, as introduced in Ref. [62]. We work in the framework of the tight-binding model, taking into account the antisymmetry of the spin–orbit coupling and chemical potential in nanowires, and obtain a more generalized condition of topological superconductivity.

Although several papers have focused on how to realize class-DIII topological superconductors in the double-quantum-wire (DQW) system [52,53,62], the relation between Kramers MFs and the odd-frequency pairing still remains largely unexplored for systems in the topological DIII class. For example, it is natural to expect that the spin structure of odd-frequency pairings in the presence of Kramers pairs is very different from that for the topological D class with a single MF. In addition, working with two quantum wires, we have to include one additional spatial degree of freedom such as the wire index. We will call the superconducting pairing wire-odd (wire-even) if the pair amplitude picks up a minus (plus) sign if one exchanges two wires. As a result, one can expect a much richer structure for the pairing amplitudes depending on the four degrees of freedom, i.e., frequency, spin, and the spatial parity inside the wire, as well as that between the two wires. Besides symmetries of Cooper pairs, the energy of Andreev bound states (ABSs) in Josephson junctions has not been addressed in this system so far.

Based on the background described in the previous paragraph, we investigate two important aspects: (i) pairing symmetry of DQWs, which hosts time-reversal symmetry: we find various types of pair amplitudes due to the translational and inversion symmetry breaking, some being unique in the DQW system. We show that, in the topological regime, the odd-frequency pairing is strongly enhanced at the ends of the system. (ii) ABSs of the Josephson junction system, which consists of DQWs: we obtain an anomalous energy dispersion of ABSs proportional to $\sim \sin\varphi$ with φ being the superconducting phase difference between the two sections. Our findings contribute to the advancement of the understanding of topological superconductivity in the DIII class and also the physics of pairing symmetry.

The remainder of the paper is organized as follows. In Sect. 2, we briefly introduce the DQW model and present its topological condition. In Sect. 3, we focus on the classification of the symmetries of Cooper pairs in DQWs and demonstrate the signatures of the emergent odd-frequency pairing states. In Sect. 4, we utilize the tunneling Hamiltonian approach to study the ABSs in the DQW/normal metal/DQW model. The Josephson effect in DQW/normal metal/spin-singlet *s*-wave superconductor junctions will be investigated as well. In Sect. 5, we summarize our results.

2. Model construction

We consider a setup consisting of two quantum wires with Rashba SOI proximity-coupled to an *s*-wave superconductor (Fig. 1). The superconductivity in the DQW system could be induced in two different ways, as described in Ref. [62]. The Cooper pair could tunnel as a whole into one of the two wires, resulting in an intrawire superconducting pairing. Alternatively, the Cooper pair

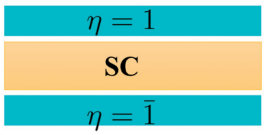

Fig. 1. A schematic picture of two Rashba QWs proximity-coupled with a superconductor (SC).

could split such that electrons tunnel into different wires, resulting in an interwire superconducting pairing, also called a crossed Andreev superconducting pairing. We will work in the framework of the tight-binding model with the Hamiltonian given by

$$\begin{aligned} H = &-t \sum_{\langle i,j\rangle\sigma\eta} c^{\dagger}_{i\sigma\eta} c_{j\sigma\eta} - \sum_{i\sigma\eta} \mu_{\eta} c^{\dagger}_{i\sigma\eta} c_{i\sigma\eta} \\ &+ i \sum_{\langle i,j\rangle\eta} \alpha_{\eta} \left(c^{\dagger}_{i\uparrow\eta} c_{j\downarrow\eta} - c^{\dagger}_{i\downarrow\eta} c_{j\uparrow\eta} \right) \\ &+ \sum_{i\eta} \Delta_{\eta} \left(c^{\dagger}_{i\uparrow\eta} c^{\dagger}_{i\downarrow\eta} + \text{H.c.} \right) \\ &+ \sum_{i} \Delta_{c} \left(c^{\dagger}_{i\uparrow 1} c^{\dagger}_{i\downarrow\bar{1}} + c^{\dagger}_{i\uparrow\bar{1}} c^{\dagger}_{i\downarrow 1} + \text{H.c.} \right). \end{aligned} \tag{1}$$

Here, we introduce index i ($\eta = 1, \bar{1}$) to label lattice sites (QWs). We define $c^{\dagger}_{i\sigma\eta}(c_{i\sigma\eta})$ as the creation (annihilation) operator acting on the electron at site i of the η QW with the spin σ ($\sigma = \uparrow\ (\equiv 1), \downarrow\ (\equiv \bar{1})$). The first term represents hopping with amplitude t between two adjacent sites $\langle i,j\rangle$. The second term describes the chemical potential μ_{η} at each site. The third term corresponds to the Rashba SOI of the amplitude α_{η}. The last two terms represent the intrawire and interwire pair potentials with amplitudes Δ_{η} and Δ_c, respectively. The interwire superconducting pairing induced by crossed Andreev processes is larger than the intrawire pairing due to strong electron–electron interactions. The crossed Andreev reflection, when two electrons initially forming the Cooper pair get separated into different channels, has attracted special attention due to its potential use for creating entanglement [63,64] and has been implemented in superconductor/normal metal/superconductor junctions [65–67] and double-quantum-dot superconductor hybrid systems [63,64,68–71]. To simplify the analytical calculations, we focus on the case of $\Delta_1 = \Delta_{\bar{1}}$ throughout this paper. Using translational invariance along the x-direction, we introduce the number of unit cells N_x and momentum in the x-direction k_x, and Fourier transform the operators as $c_{i\sigma\eta} = \frac{1}{\sqrt{N_x}} \sum_{k_x} e^{ik_x a_x i} c_{k_x\sigma\eta}$. The Hamiltonian can be rewritten in the momentum representation in the basis composed of $c_{k_x} = (c_{k_x\uparrow 1}, c_{k_x\downarrow 1}, c_{k_x\uparrow\bar{1}}, c_{k_x\downarrow\bar{1}}, c^{\dagger}_{-k_x\uparrow 1}, c^{\dagger}_{-k_x\downarrow 1}, c^{\dagger}_{-k_x\uparrow\bar{1}}, c^{\dagger}_{-k_x\downarrow\bar{1}})^T$ as

$$\begin{aligned} \mathcal{H}(k_x) = &\left[\frac{\xi_{k_x 1}}{2} \tau_z + \alpha_1 \sin(k_x a_x) \tau_z s_y \right] (1 + \eta_z) \\ &+ \left[\frac{\xi_{k_x \bar{1}}}{2} \tau_z + \alpha_{\bar{1}} \sin(k_x a_x) \tau_z s_y \right] (1 - \eta_z) \\ &- \Delta_1 \tau_y s_y - \Delta_c \tau_y s_y \eta_x. \end{aligned} \tag{2}$$

Here, $s_{x,y,z}$, $\tau_{x,y,z}$, and $\eta_{x,y,z}$ are Pauli matrices acting on the degree of freedom of spin, particle–hole, and chain, respectively. We define $\xi_{k_x\eta}$ as $\xi_{k_x\eta} = -2t\cos(k_x a_x) - \mu_{\eta}$.

By linearizing the energy spectrum [72], the authors of Ref. [62] found that, when $\Delta_c > \Delta_1$, a time-reversal invariant topological superconductor is realized. Here, we study this setup by tight-binding analysis to find whether the time-reversal invariant topological superconductor is obtained beyond the linearized approximation of the energy dispersion. As opposed to the previous study [62], we will find that the antisymmetric parameters defined in Eq. (5) play a crucial role for the realization of class-DIII superconductivity. Based on the "weak pairing limit", we can define the topological condition as follows:

$$(-1)^{\nu} = \prod_{k_x=k_{F,1},k_{F,2}} \mathrm{sgn}[\Delta_c^2 - \Delta_1^2 - (\mu_a + 2\alpha_a \sin k_x a_x)^2], \tag{3}$$

where for $\nu = 1(0)$ the system is in a nontrivial (trivial) topological state, and $k_{F,1}$ and $k_{F,2}$ are defined such that

$$2\Delta_1(2t\cos k_x a_x + 2\alpha_s \sin k_x a_x + \mu_s) = 0 \tag{4}$$

at $k_x = k_{F,1}, k_{F,2}$ with

$$\begin{aligned} \alpha_{s/a} &= (\alpha_1 \pm \alpha_{\bar{1}})/2, \\ \mu_{s/a} &= (\mu_1 \pm \mu_{\bar{1}})/2. \end{aligned} \tag{5}$$

For a more detailed derivation of the topological condition, see Appendix A.

First, we note from Eq. (3) that the condition $\Delta_c > \Delta_1$ has to be satisfied to realize a topologically nontrivial state, otherwise the product in Eq. (3) is always positive and the system is in the trivial state. Also, α_a should not be nonzero because only the term $\alpha_a \sin k_x a_x$ can produce the sign change of $[\Delta_c^2 - \Delta_1^2 - (\mu_a + 2\alpha_a \sin k_x a_x)^2]$, which leads to the minus sign of the product. Thus, the antisymmetric SOI is crucial for inducing the topologically nontrivial state. Otherwise, the SOI could be gauged away, as was noted in Refs. [62,74].

To get the explicit phase diagram for the system, we consider a simplified case by setting $\alpha_s = 0$. In this case, the Fermi points $k_{F,1}$ and $k_{F,2}$ are defined via

$$\varepsilon(k_x) = -2t\cos k_x a_x - \mu_s = 0, \tag{6}$$

and are given by

$$k_{F,1}a_x = -\arcsin[\mu_0],\ k_{F,2}a_x = \arcsin[\mu_0] \tag{7}$$

with $\mu_0 \equiv \sqrt{1-(\mu_s/2t)^2}$ for $|\mu_s| < 2t$. According to Eq. (3),

$$\begin{aligned} (-1)^{\nu} = \mathrm{sgn}\Big[&\Delta_c^2 - \Delta_1^2 - (\mu_a + 2\alpha_a\mu_0)^2] \\ &\times \mathrm{sgn}\Big[\Delta_c^2 - \Delta_1^2 - (\mu_a - 2\alpha_a\mu_0)^2\Big] \end{aligned} \tag{8}$$

has to result in $\nu = -1$ to realize the topological phase. For $\alpha_a\mu_a > 0$, Eq. (8) is equivalent to

$$|\mu_a + 2\alpha_a\mu_0| > \sqrt{\Delta_c^2 - \Delta_1^2} > |\mu_a - 2\alpha_a\mu_0|, \tag{9}$$

which has to be satisfied in order to get the nontrivial state. The result of Eq. (9) is consistent with Refs. [53,62]. In Fig. 2(a) (2(b)), we show the phase diagram of the DQW system as a function of

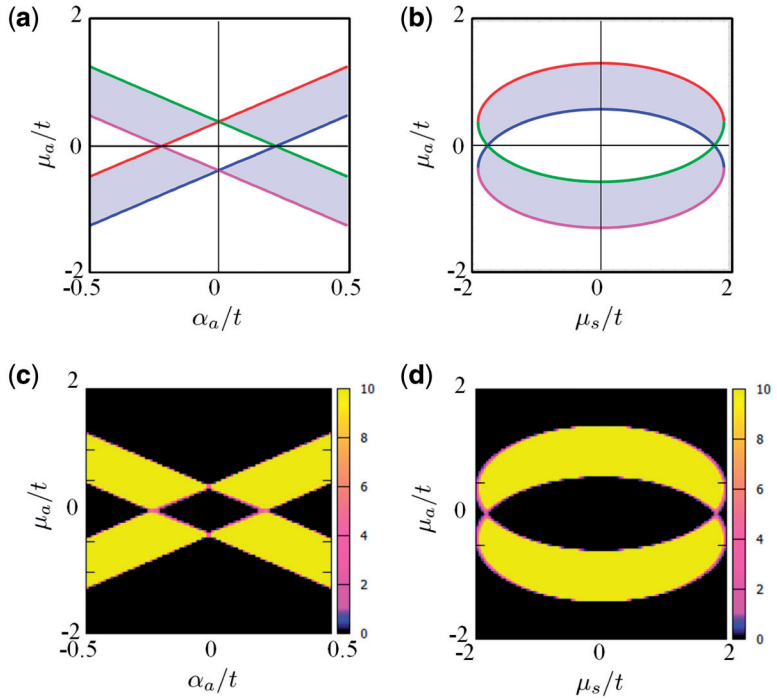

Fig. 2. (a) ((b)) Topological phase diagram of the DQW model as a function of α_a and μ_a (μ_s and μ_a) with $\Delta_c/t = 0.4$, $\Delta_1/t = 0.1$, and $\mu_s/t = -1$ ($\Delta_c/t = 0.4$, $\Delta_1/t = 0.1$, and $\alpha_a/t = 0.5$). The light gray area represents the topologically nontrivial phase. The red, green, blue, and magenta lines correspond to $\mu_a = 2\alpha_a\mu_0 + \sqrt{\Delta_c^2 - \Delta_1^2}$, $\mu_a = -2\alpha_a\mu_0 + \sqrt{\Delta_c^2 - \Delta_1^2}$, $\mu_a = 2\alpha_a\mu_0 - \sqrt{\Delta_c^2 - \Delta_1^2}$, and $\mu_a = -2\alpha_a\mu_0 - \sqrt{\Delta_c^2 - \Delta_1^2}$, respectively. (c) ((d)) The intensity plot of LDOS of zero energy on the edge of the DQW model found by the recursive Green's function technique as a function of α_a and μ_a (μ_s and μ_a) with $\Delta_c/t = 0.4$, $\Delta_1/t = 0.1$, and $\mu_s/t = -1$ ($\Delta_c/t = 0.4$, $\Delta_1/t = 0.1$, and $\alpha_a/t = 0.5$). We define LDOS as $\rho \equiv -\frac{1}{\pi}\mathrm{ImTr}[G]$, where G is determined recursively utilizing H in Eq. (1). For the more detailed derivation, see Ref. [24]. We set the length of the system long enough (4000 sites) so that overlapping between zero-energy states on both edges is negligible [73]. Note that the nontrivial area in (a) and (b) corresponds well to that of the large amplitude of LDOS in (c) and (d).

α_a and μ_a (μ_s and μ_a) with fixed Δ_c, Δ_1, and μ_s (Δ_c, Δ_1, and α_a). The obtained results are in good agreement with the results obtained in the tight-binding framework, as the nonzero LDOS at zero energy on the edge of the DQW system indicates; see Figs. 2(c) and 2(d).

To summarize this section, two conditions, $\Delta_c > \Delta_1$ and $\alpha_a \neq 0$, are necessary but not sufficient to generate time-reversal invariant topological superconductivity. As we show in the next section, the presence of the zero-energy state also changes the dominant symmetries of Cooper pairs at the end of the system.

3. Cooper-pair symmetry

In this section, we study symmetries of Cooper pairs in the model of the double Rashba QW system coupled to an s-wave superconductor. In addition to the standard symmetries of Cooper pairs, where frequency, spin, and parity are taken into account, we should include one more spatial degree of freedom connecting to two QWs. We call the pair amplitude wire-odd (wire-even) if it picks up a negative sign (remains the same) by the exchange of the wire index. Due to this additional degree of freedom, there are now eight classes of Cooper pair with different symmetries that are consistent with Fermi–Dirac statistics, as summarized in Table 1. These classes are i) even-frequency spin-singlet

Table 1. All possible symmetries of Cooper pairs occurring in the double-QW system.

	Frequency	Spin	Parity	Wire	Total
ESEE	+(Even)	−(Singlet)	+(Even)	+(Even)	−(Odd)
ESOO	+(Even)	−(Singlet)	−(Odd)	−(Odd)	−(Odd)
ETOE	+(Even)	+(Triplet)	−(Odd)	+(Even)	−(Odd)
ETEO	+(Even)	+(Triplet)	+(Even)	−(Odd)	−(Odd)
OSOE	−(Odd)	−(Singlet)	−(Odd)	+(Even)	−(Odd)
OSEO	−(Odd)	−(Singlet)	+(Even)	−(Odd)	−(Odd)
OTEE	−(Odd)	+(Triplet)	+(Even)	+(Even)	−(Odd)
OTOO	−(Odd)	+(Triplet)	−(Odd)	−(Odd)	−(Odd)

even-parity even-wire (ESEE), ii) even-frequency spin-singlet odd-parity odd-wire (ESOO), iii) even-frequency spin-triplet odd-parity even-wire (ETOE), iv) even-frequency spin-triplet even-parity odd-wire (ETEO), v) odd-frequency spin-singlet odd-parity even-wire (OSOE), vi) odd-frequency spin-singlet even-parity odd-wire (OSEO), vii) odd-frequency spin-triplet even-parity even-wire (OTEE), and viii) odd-frequency spin-triplet odd-parity odd-wire (OTOO). The generation of Cooper pairs with odd-wire symmetry, i.e., ESOO, ETEO, OTOO, and OSEO symmetry, is a remarkable feature of this model.

In the following, we discuss how to evaluate pair amplitudes of various symmetries. Using Eq. (1), we define the Matsubara Green's function as follows:

$$G_M(\omega_n,j,j',\sigma,\sigma',\eta,\eta') = \left(\frac{1}{i\omega_n - H}\right)_{j,j',\sigma,\sigma',\eta,\eta'} \tag{10}$$

with the Matsubara frequency, which is set to be $\omega_n/t = 0.01$ throughout the paper without loss of generality. Introducing matrices $G(\omega_n,j,j',\sigma,\sigma',\eta,\eta')$ and $F(\omega_n,j,j',\sigma,\sigma',\eta,\eta')$, we rewrite Eq. (10) as

$$G_M = \begin{pmatrix} G & F \\ \tilde{F} & \tilde{G} \end{pmatrix}, \tag{11}$$

where G_M is divided into four sectors in the particle–hole space. We focus on $F(\omega_n,j,j',\sigma,\sigma',\eta,\eta')$ to analyze the symmetries of Cooper pairs. First, we focus on the frequency dependence. Introducing $J \equiv (j,j',\sigma,\sigma',\eta,\eta')$, we define $F_{\rm O}(J)$ and $F_{\rm E}(J)$ as follows:

$$F_{\mathfrak{A}}(J) = \frac{F(\omega_n;J) + {\rm sgn}[\mathfrak{A}]F(-\omega_n;J)}{2}. \tag{12}$$

Here, we define $\mathfrak{A} = {\rm E}, {\rm O}$ with the convention that ${\rm sgn}[{\rm E/O}] = \pm 1$. Then, using Eq. (12) and defining K as $K \equiv (\sigma,\sigma',\eta,\eta')$, we introduce $F_{\rm OO}(j;K), F_{\rm OE}(j;K), F_{\rm EO}(j;K)$, and $F_{\rm EE}(j;K)$, also classified by the spatial symmetry inside the QW as

$$\begin{aligned} F_{\mathfrak{AB}}(j;K) = \frac{1}{2}\Big\{ & F_{\mathfrak{A}}\left(j + \frac{1-{\rm sgn}[\mathfrak{B}]}{2}, j\right) \\ & + {\rm sgn}[\mathfrak{B}] F_{\mathfrak{A}}\left(j, j + \frac{1-{\rm sgn}[\mathfrak{B}]}{2}\right)\Big\}, \end{aligned} \tag{13}$$

with $\mathfrak{B} = \mathrm{E}, \mathrm{O}$. Further, by denoting L as $L \equiv (\sigma, \sigma')$, we can address the spatial symmetry between QWs defined by $F_{\mathfrak{AB}\mathrm{O}}(j;L)$, $F_{\mathfrak{AB}\mathrm{E}}(j;L)$ as

$$F_{\mathfrak{AB}\mathfrak{C}}(j;L) = \frac{F_{\mathfrak{AB}}(j;L;1,\bar{1}) + \mathrm{sgn}[\mathfrak{C}]F_{\mathfrak{AB}}(j;L;\bar{1},1)}{2}, \tag{14}$$

with $\mathfrak{C} = \mathrm{E}, \mathrm{O}$. Finally, by also addressing the spin degree of freedom, we get eight classes of pair amplitude, which are given by

$$F^{\uparrow\downarrow}_{\mathfrak{A}\mathrm{T}\mathfrak{B}\mathfrak{C}}(j) = \frac{F_{\mathfrak{AB}\mathfrak{C}}(j;\uparrow,\downarrow) + F_{\mathfrak{AB}\mathfrak{C}}(j;\downarrow,\uparrow)}{2} \tag{15}$$

$$F_{\mathfrak{A}\mathrm{S}\mathfrak{B}\mathfrak{C}}(j) = \frac{F_{\mathfrak{AB}\mathfrak{C}}(j;\uparrow,\downarrow) - F_{\mathfrak{AB}\mathfrak{C}}(j;\downarrow,\uparrow)}{2}, \tag{16}$$

where the indices $\mathfrak{A}, \mathfrak{B}$, and $\mathfrak{C}$ take values of either E or O. The combination of $\mathfrak{A}, \mathfrak{B}$, and $\mathfrak{C}$ has to satisfy

$$\mathrm{sgn}[\mathfrak{A}]\mathrm{sgn}[\mathfrak{B}]\mathrm{sgn}[\mathfrak{C}] = -1(+1) \tag{17}$$

for the spin-triplet (spin-singlet) pairing. As for the $\uparrow\uparrow$ and $\downarrow\downarrow$ spin-triplet components, the corresponding pair amplitudes are

$$F^{\uparrow\uparrow}_{\mathfrak{A}\mathrm{T}\mathfrak{B}\mathfrak{C}}(j) = F_{\mathfrak{A}\mathrm{T}\mathfrak{B}\mathfrak{C}}(j,\uparrow,\uparrow) \tag{18}$$

$$F^{\downarrow\downarrow}_{\mathfrak{A}\mathrm{T}\mathfrak{B}\mathfrak{C}}(j) = F_{\mathfrak{A}\mathrm{T}\mathfrak{B}\mathfrak{C}}(j,\downarrow,\downarrow). \tag{19}$$

We emphasize that, due to the time-reversal symmetry present in the system, the $\uparrow\downarrow$ components of the spin-triplet are absent. Indeed, using the definition of the anomalous Green's function,

$$F^{\dagger}(\omega_n, j, j', \sigma, \sigma', \eta, \eta') \equiv \int_0^\beta d\tau e^{i\omega_n\tau} \left\langle c^\dagger(\tau)_{j,\sigma,\eta} c^\dagger(0)_{j',\sigma',\eta'} \right\rangle, \tag{20}$$

$$F(\omega_n, j, j', \sigma, \sigma', \eta, \eta') \equiv \int_0^\beta d\tau e^{i\omega_n\tau} \left\langle c(\tau)_{j,\sigma,\eta} c(0)_{j',\sigma',\eta'} \right\rangle, \tag{21}$$

with imaginary time τ and inverse temperature $\beta = 1/k_B T$, as well as the fact that

$$c(\tau)_{j,\uparrow,\eta} \xrightarrow{\mathfrak{T}} -c(\tau)_{j,\downarrow,\eta} \tag{22}$$

$$c(\tau)_{j,\downarrow,\eta} \xrightarrow{\mathfrak{T}} c(\tau)_{j,\uparrow,\eta} \tag{23}$$

under time-reversal operation $\mathfrak{T}$, we obtain

$$\begin{aligned} &\mathfrak{T}[F(M;\uparrow,\downarrow;N) + F(M;\downarrow,\uparrow;N)]\mathfrak{T}^{-1} \\ &= -[F(M'\downarrow,\uparrow;N) + F(M'\uparrow,\downarrow;N)] \end{aligned} \tag{24}$$

for the time-reversal invariant system. Using the fact that the Green's function in Eq. (11) is invariant under the time-reversal operation, we conclude that the $\uparrow\downarrow$ components of the spin-triplet are absent. Above, we have used the notations $M \equiv (\omega_n, j, j')$, $M' \equiv (-\omega_n, j, j')$, and $N \equiv (\eta, \eta')$. By a similar argument, we show that the $\uparrow\uparrow$ and $\downarrow\downarrow$ components are equal.

Equations (15)–(19) describe all possible types of pair amplitudes; these are also represented in Table 1.

The odd-frequency pairings combined with even-wire symmetry cases, v) and vii), have been studied in previous work dedicated to ferromagnet junctions, unconventional superconductor junctions, and nonuniform superconducting systems [9,37–40,75–78]. The odd-frequency pairings combined with odd-wire symmetry, vi) and viii), are similar to pairings with odd-wire symmetry in bulk multiband (orbital) systems [79–82] and those with odd-channel symmetry in the two-channel Kondo lattice model [83]. In contrast to the previous relevant cases, the magnitude of odd-wire pairings can be enhanced at the edge in the topological regime in the present model.

Before we begin the numerical calculations, we clarify the general properties of the Hamiltonian and resulting symmetries of pairing amplitudes. First, we consider the infinite DQW model. We start from the case with $\mu_a = 0$, $\alpha_s = 0$, and $\alpha_a = 0$. In this case, only the ESEE pairing is present. This is the standard pairing for Δ_1 and Δ_c originating from an s-wave superconductor without any symmetry breaking in double-wire and spin-rotational spaces as well as without breaking of the translational invariance. As shown in Table 2, by breaking these symmetries, seven additional types of superconducting pairing are induced. In case (1), we break only the double-wire symmetry by adding nonzero μ_a. Now, the double-wire-even and double-wire-odd pairings can mix without changing symmetries in the spin space and without breaking the translational invariance. To be consistent with Fermi–Dirac statistics, the parity in the frequency space should be switched; thus, the OSEO pairing is induced. In case (2), only α_s is chosen to be nonzero; thus, the spin rotational symmetry and spatial parity inside the wire are broken at the same time. Then, the ETOE pairing is induced without generating the odd-frequency pairing, as was shown before in noncentrosymmetric superconductors with Rashba SOI [84]. Next, in case (3), the induced symmetries can be understood by combining the results of cases (1) and (2). In addition to the ESEE pairing, the OTOO, OSEO, ETOE pairings are induced by the coexistence of μ_a and α_s. We note that the presence of asymmetric Rashba coupling α_a also corresponds to case (3), as it breaks the double-wire symmetry and plays a role similar to α_s in the spin space.

Table 2. The eight classes of possible symmetries of Cooper pairs in the DQW system. The classes are characterized by broken symmetries. The symmetry between two QWs comprising the DQW system could be broken by detuning of the chemical potential. The spin space symmetry could be broken by the SOI. The translational invariance is broken, e.g., by boundary conditions. The label ◯ (–) indicates that the symmetry is broken (preserved).

	Broken symmetry			
	DQW μ_a	spin α_s	translation boundary	Pairing symmetry
(0)	–	–	–	ESEE
(1)	◯	–	–	ESEE, OSEO
(2)	–	◯	–	ESEE, ETOE
(3)	◯	◯	–	ESEE, OSEO, ETOE, OTOO
(4)	–	–	◯	ESEE, OSOE
(5)	◯	–	◯	ESEE, OSEO, OSOE, ESOO
(6)	–	◯	◯	ESEE, ETOE, OSOE, OTEE
(7)	◯	◯	◯	ESEE, OSEO, ETOE, OTOO OSOE, ESOO, OTEE, ETEO

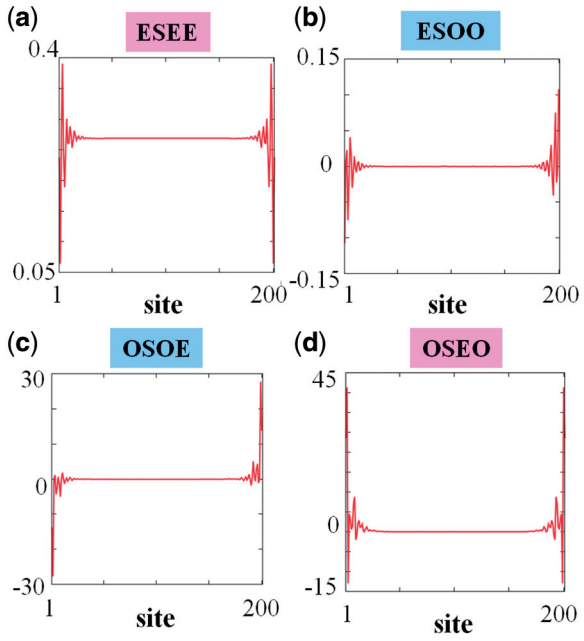

Fig. 3. The spatial profiles of four singlet pairing amplitudes (denoted above each figure) for a DQW system of a finite size of 200 sites. The parameters are set as follows: $\alpha_1/t = -\alpha_{\bar{1}}/t = 0.5$, $\mu_1/t = -2$, $\mu_{\bar{1}}/t = -1$, $\Delta_1/t = 0.1$, and $\Delta_c/t = 0.4$. We confirm that the odd-frequency pairing amplitudes are strongly enhanced at both edges, as panels (c) and (d) show.

Next, we consider systems in which the translation invariance is also broken, e.g., if some parameters are nonuniform or the system is finite. Thus, parity mixing can occur by reversing the parity corresponding to the frequency [9,37,39] to be consistent with Fermi–Dirac statistics. We first consider the case of $\mu_s = 0$ and $\alpha_s = 0$. In case (4), the breakdown of the parity inside a wire induces the OSOE pairing. This result is consistent with preexisting results in nonuniform superconducting systems [9,37,39,85]. The induced pairings obtained in case (5) can be understood by combining the results of cases (1) and (4). The ESOO pairing is induced by the breakdown of the translational invariance and the double-wire symmetry. Also, the results in case (6) can be understood by combining the results in cases (2) and (4). The OTEE pairing is induced from the ETOE pairing by breaking of the translation invariance. The most interesting situation is case (7). The OSEO, ETOE, and OTOO pairings stem from the results in case (3). Similar to case (4), the OSOE, ESOO, OTEE, and ETEO pairings are generated by the spatial parity mixing due to the fact that the translation invariance is broken.

We calculate the spatial profiles of pairing amplitudes numerically for parameters chosen such that the system is in the topological regime; see Figs. 3 and 4. First, the odd-frequency components, i.e., the magnitudes of the pairing amplitudes of OSEO, OTOO, OSOE, and OTEE, are hugely enhanced (more explicitly, the ratios of OSEO, OTOO, OSOE, and OTEE to ESEE are of the order of $\sim 10^2$) at the system edge, consistent with the existence of the zero-energy state, i.e., Kramers Majorana fermions, similar to the previous results obtained in unconventional superconductors [37–39]. Second, in addition to the ESEE pairing, which is the primary symmetry of the parent system (see Fig. 3(a)), the ETOE pairing spreads over the system (see Fig. 4(a)). Although the OTOO and OSEO pairings are possible in the bulk from the discussion of the pairing symmetries (see above in Table 2), their magnitudes are small. The ESOO and ETEO pairing strengths are small (the ratios of ESOO and ETEO to ESEE are of the order of $\sim 10^0$) and nonzero only at the system

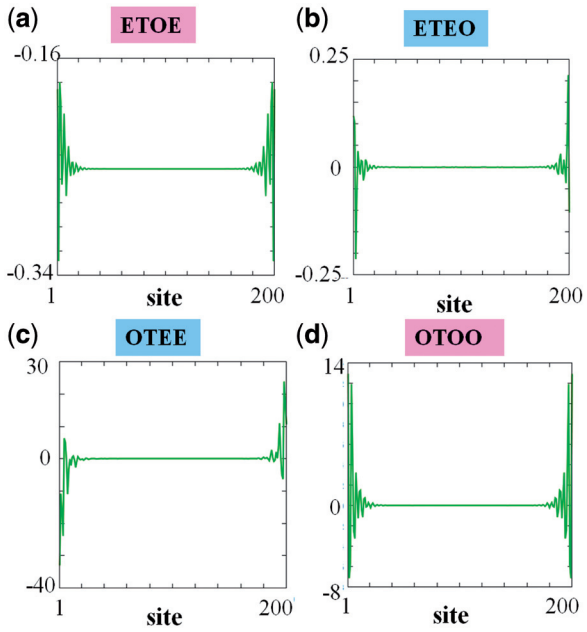

Fig. 4. The spatial profiles of four triplet pairing amplitudes. The parameters are the same as in Fig. 3. Again, the odd-frequency pairing amplitudes peak at the edges, where Kramers pairs of MFs are located; see panels (c) and (d).

edge due to the breakdown of translational symmetry. To understand the spatial profiles of these pairing amplitudes, it is convenient to focus on the inversion parity of the pairing amplitudes around the center of the quantum wire. As seen from Figs. 3 and 4, the inversion parity is even for the ESEE, OSEO, ETOE, OTOO pairings. These pairings can also exist in the bulk. In contrast to this, the inversion parities of the OSOE, ESOO, OTEE, ETEO pairings are odd. They are generated due to the breakdown of the translational invariance and are localized at the edges.

To emphasize the correspondence between zero-energy states and odd-frequency pairings explicitly, we calculated numerically the LDOS at the edge of the DQW system and the pairing amplitudes of OSEO and OTEE (see Fig. 5) for three different cases. The pairing amplitudes (see Figs. 5(b)–(e)) change as a function of energy similar to the LDOS (see Fig. 5(a)). Specifically, when the parameters are set to satisfy the topological criterion (blue line in Fig. 5), the real parts of the OSEO and OTEE pairing amplitudes change abruptly around zero energy. Importantly, the imaginary parts of the OSEO and OTEE pairing amplitudes peak strongly at zero energy, confirming the connection between the presence of the MFs and the odd-frequency pairing.

4. Josephson junction of DQWs

In this section, we address Andreev bound states (ABSs) in DQW/DQW junctions. The ABSs localized between two superconductors have been extensively studied in the literature. The energy of the ABS E_b localized between two topologically trivial s-wave superconductors is given by $E_b = \pm\sqrt{1 - \sigma_N \sin^2(\varphi/2)}\Delta_0$, where Δ_0, φ, and σ_N are the magnitude of the superconducting pairing potential, the phase difference between superconductors, and the transparency of the junctions, respectively [86]. On the other hand, the energy of ABS E_b between two 1D topological p_x-wave superconductors is given by $E_b = \pm\sqrt{\sigma_N}\Delta_0 \cos\varphi/2$ [87,88]. A similar result is also known from the study of d-wave superconductor junctions [7,89]. The present anomalous φ dependence of the ABS

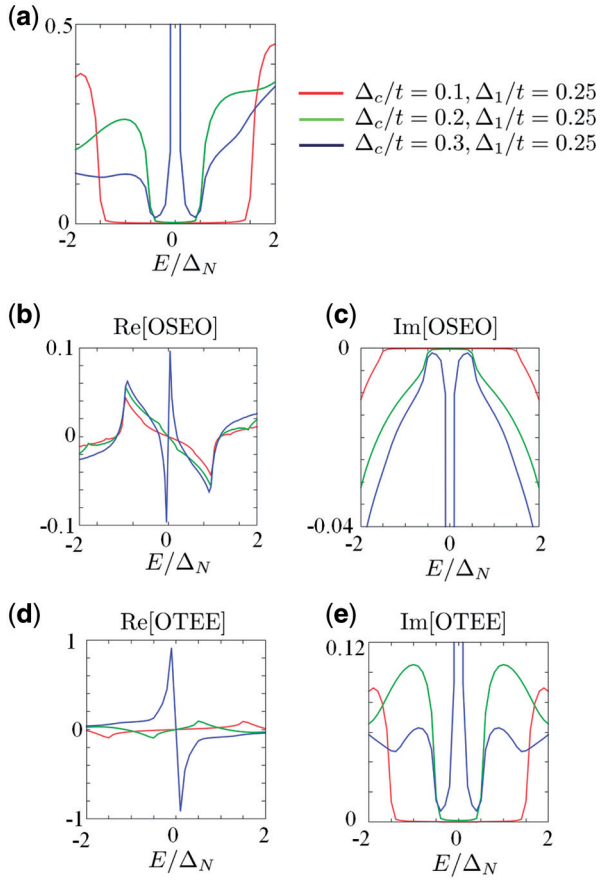

Fig. 5. (a) The LDOS on the edge of a DQW system of a length of 4000 sites. (b), (c) The real and imaginary parts of the OSEO pairing. (d), (e) The real and imaginary parts of the OTEE pairing. Plots are based on the recursive Green's function technique. The parameters are set as follows: $\alpha_1/t = -\alpha_{\bar{1}}/t = 0.5$, $\mu_1/t = -2$, and $\mu_{\bar{1}}/t = -1$.

can be explained by the coupling of MFs on both sides in the Kitaev chain/Kitaev chain Josephson junction system [88]. It also generates 4π periodicity of the AC Josephson current in the Josephson junctions based on topological superconductors. In this section, we calculate the energy of the ABSs and find anomalous $\sim \pm \sin\varphi$ dependence. We provide a qualitative explanation of this sinusoidal curve by considering the coupling of the Kramers pair of MFs to an s-wave superconductor. We also construct an effective model, which address the $s + p/s$-wave superconductor junctions, to explain this phase dependence of the ABS energy.

Making use of the recursive Green's function technique, we can calculate the spectrum and the energy of the ABSs. First, we focus on the case when both sides of the DQWs are in the nontrivial topological regime. The result is shown in Fig. 6(a). This behavior is similar to the case of the Kitaev chain/Kitaev chain or p-wave/p-wave junction system, which demonstrates [88] $\sim \pm\cos\varphi/2$. By introducing $\gamma_\uparrow$ and $\gamma_\downarrow$ to describe two different MFs making up the Kramers pair, we can understand the curve in Fig. 6(a) by the coupling of $\gamma_\uparrow$ and $\gamma_\downarrow$ on both sides, analogously to the above-mentioned Kitaev chain/Kitaev chain junction. If the sign of the Rashba SOI is reversed on the right-hand side, the spectrum of the ABSs is trivially shifted by π, as shown in Fig. 6(b). This is an example of the so-called 0-π transition: by reversing the sign of the Rashba term, the phase of the effective p-wave superconductor is flipped by π. This transition has already been discussed in the system of a Rashba quantum wire on a superconductor with applied Zeeman fields, where topological superconductivity

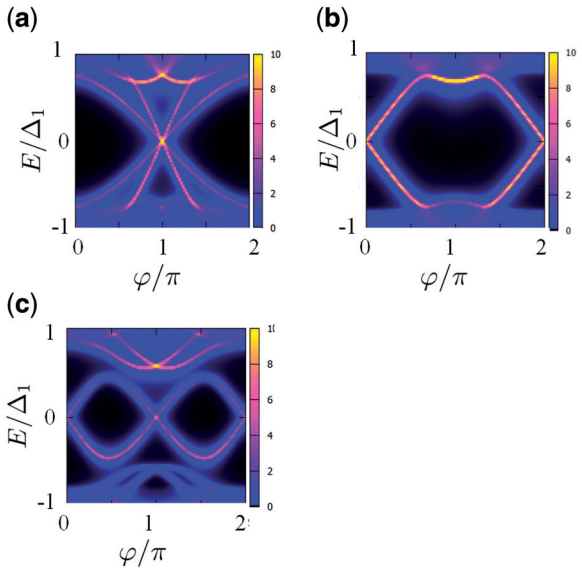

Fig. 6. (a) The spectrum of the ABSs in the DQW/normal metal/DQW junction as a function of the phase difference φ. The parameters are set to be the same on both sides and correspond to the topologically nontrivial regime: $\alpha_1/t = -\alpha_{\bar{1}}/t = 0.5$, $\mu_1/t = -2$, $\mu_{\bar{1}}/t = -1$, $\Delta_1/t = 0.1$, and $\Delta_c/t = 0.4$. The ABSs behave like $\sim \pm\cos\varphi/2$. (b) Next, we reverse the signs of the Rashba SOI on the right-hand side, i.e., $\alpha_1/t = -\alpha_{\bar{1}}/t = -0.5$; the other parameters are set to be the same as in panel (a). The ABSs exhibit a π-shift and their energy behaves like $\sim \pm\sin\varphi/2$. (c) The right-hand side of the system is brought into the trivial regime with the parameters chosen as $\alpha_1/t = \alpha_{\bar{1}}/t = 0$, $\mu_1/t = -1$, $\mu_{\bar{1}}/t = -1$, and $\Delta_1/t = 0.1$. The ABSs near the Fermi energy level behave like $\sim \pm\sin\varphi$. For all panels, the calculation is based on the recursive Green's function technique, and we set the length of the right and left superconducting sections (normal metal section) to 4000 (2) lattice sites. The chemical potential in the normal section is set to $\mu_N/t = -1$.

of class D is realized [90–92]. Indeed, the observed behavior (see Fig. 6(b)) can also be explained by the above-mentioned transition using the effective model of DQWs discussed below.

Next, we check the most interesting regime in which we set one side of the junction to be in the topological regime and the other to be in the trivial regime (see Fig. 6(c)). The energy spectrum of the ABSs follows $\sim \pm\sin\varphi$. This feature can be explained by the coupling of Kramers pair of MFs and to the *s*-wave superconductor, as we demonstrate below.

The tunneling Hamiltonian can be written as

$$H_T = \sum_{k\sigma}\Big(T_k\gamma_\sigma b_{k\sigma} + \text{h.c.}\Big), \tag{25}$$

where T_k is the tunneling amplitude, $b_{k\sigma}$ is the annihilation operator acting on the electron on the right-hand side of the junction with spin σ and momentum k. The Majorana operator γ_σ acts on the left-hand side of the junction with the index σ used to distinguish between two MFs building a Kramers pair. We introduce the Bogoliubov transformation as follows:

$$\begin{aligned} b_{k\uparrow} &= u_k\alpha_{k\uparrow} + v_k^*\alpha_{-k\downarrow}^\dagger \\ b_{k\downarrow} &= u_{-k}\alpha_{k\downarrow} - v_{-k}^*\alpha_{-k\uparrow}^\dagger, \end{aligned} \tag{26}$$

where u_k and v_k are given by

$$u_k = \frac{1}{2}\sqrt{1+\frac{\xi_k}{E_k}},\quad v_k = \frac{1}{2}\sqrt{1-\frac{\xi_k}{E_k}}\exp(i\varphi),$$

and φ is the macroscopic phase difference between the right and left superconductors. Here, ξ_k is the energy spectrum of the right superconductor in the normal state and $E_k = \sqrt{\xi_k^2 + |\Delta_k|^2}$ is the quasiparticle energy spectrum, where Δ_k is the pair potential in the right-hand side superconductor. Without loss of generality, u_k can be set to be a real number and v_k a complex number. As a result, the tunneling Hamiltonian is rewritten as

$$H_T = \sum_k \Big\{ T_k \gamma_\uparrow (u_k \alpha_{k\uparrow} + v_k^* \alpha_{-k\downarrow}^\dagger) + T_k^* (u_k \alpha_{k\uparrow}^\dagger + v_k \alpha_{-k\downarrow}) \gamma_\uparrow$$
$$+ T_k \gamma_\downarrow (u_{-k} \alpha_{k\downarrow} - v_{-k}^* \alpha_{-k\uparrow}^\dagger) + T_k^* (u_{-k} \alpha_{k\downarrow}^\dagger - v_{-k} \alpha_{-k\uparrow}) \gamma_\downarrow \Big\}. \tag{27}$$

At the next step, we construct the effective Hamiltonian describing the coupling between two MFs in the second order perturbation theory,

$$H_{\rm MF} = \langle 0 | H_T \frac{1}{E - H_0} H_T | 0 \rangle , \tag{28}$$

where H_0 represents the Bogoliubov–de Gennes (BdG) Hamiltonian *without* tunneling (25), $H_0 \equiv \sum_{k\sigma} E_k \alpha_{k\sigma}^\dagger \alpha_{k\sigma}$, and $|0\rangle$ is set to be the ground state of the quasiparticles. From Eq. (28), one finds

$$H_T |0\rangle = \sum_k (T_k v_k \gamma_\uparrow \alpha_{-k\downarrow}^\dagger - T_k^* u_k \gamma_\uparrow \alpha_{k\uparrow}^\dagger - T_k v_{-k} \gamma_\downarrow \alpha_{-k\uparrow}^\dagger - T_k^* u_{-k} \gamma_\downarrow \alpha_{k\downarrow}^\dagger) |0\rangle , \tag{29}$$

$$\langle 0 | H_T = \langle 0 | \sum_{k'} (T_{k'}^* v_{k'}^* \alpha_{-k'\downarrow} \gamma_\uparrow - T_{k'} u_{k'} \alpha_{k'\uparrow} \gamma_\uparrow - T_{k'}^* v_{-k'\uparrow}^* \alpha_{-k'} \gamma_\downarrow - T_{k'} u_{-k'} \alpha_{k'\downarrow}^\dagger \gamma_\downarrow), \tag{30}$$

$$H_{\rm MF} = -\sum_k \frac{|T_k|^2}{E_k} \Big\{ 2u_k^2 + 2|v_k|^2 + \Big(\frac{\Delta_k}{2E_k} - \frac{\Delta_k^*}{2E_k}\Big) \gamma_\uparrow \gamma_\downarrow - \Big(\frac{\Delta_k}{2E_k} - \frac{\Delta_k^*}{2E_k}\Big) \gamma_\downarrow \gamma_\uparrow \Big\}. \tag{31}$$

Here, we have used the fact that $u_k = u_{-k}$, $v_k = v_{-k}^*$, and $T_k = T_{-k}^*$, and also set $E = 0$. First, we ignore the first two terms in Eq. (31) because they are constant by noting $u_k^2 + |v_k|^2 = 1$. If we impose a phase difference between the left and right superconductors of $\Delta_k \to \bar{\Delta}_0 e^{i\varphi}$, $H_{\rm MF}$ can be written in the basis of $(\gamma_\uparrow, \gamma_\downarrow)^T$ as

$$H_{\rm MF} = \sum_k \bar{\Delta}_0 \frac{|T_k|^2}{E_k^2} \sin\varphi \begin{pmatrix} 0 & -i \\ i & 0 \end{pmatrix} \tag{32}$$

with the energies given by $\pm \frac{|T_k|^2}{E_k^2} \bar{\Delta}_0 \sin\varphi$, which coincides with the dispersion relation obtained for the ABSs in Fig. 6(c). This relation was also provided in Ref. [93]. Further, the ABS with $\sin\varphi$ dependence was previously predicted in a junction between a noncentrosymmetric superconductor and a conventional s-wave superconductor [94].

The characteristic features of the energy dispersion of the ABSs shown in Fig. 6(c) are also reproduced by the quasiclassical theory based on the effective model discussed in Ref. [53]. Following Ref. [53], we treat the terms breaking the symmetry between QWs as perturbations. Converting the lattice model back to a continuous one, the effective Hamiltonian is written as

$$\mathcal{H}_{qk} = (\frac{\hbar^2 k_x^2}{2m} - 2t - \mu_s)\tau_z - (\Delta_s + k_x s_y \Delta_p) s_y \tau_y, \tag{33}$$

$$\Delta_s = \Delta_1 - \Delta_c + \frac{\mu_a^2 + k_x^2 \alpha_a^2}{\Delta_1 + \Delta_c}, \tag{34}$$

$$\Delta_p = 2\frac{\alpha_a \mu_a}{\Delta_1 + \Delta_c}, \tag{35}$$

where m is the effective mass given by $m = \hbar^2/2ta_x^2$. As seen from Eq. (35), if the signs of Rashba SOI are reversed, the phase of the effective p-wave pair potential is shifted by π, which explains the 0–π transition in Fig. 6(b). For simplicity, we set the s-wave pair potential to be determined at the Fermi momentum:

$$\begin{aligned}\Delta_s &= \Delta_1 - \Delta_c + \frac{\mu_a^2 + k_F^2\alpha_a^2}{\Delta_1 + \Delta_c} \\ &= \Delta_1 - \Delta_c + \frac{\mu_a^2 + 2m(2t + \mu_s)\alpha_a^2}{\Delta_1 + \Delta_c}.\end{aligned} \tag{36}$$

If we set $\Delta_p > \Delta_s/\sqrt{2m(2t + \mu_s)}$, time-reversal topological superconductivity is realized [53]. The effective Hamiltonian describes a 1D s+p-wave superconductor. Generally, it is known that, if the p-wave component of the pair potential is larger than the s-wave component, a topological superconductor hosting edge states is realized [95].

Next, we show that the behavior of ABSs obtained in Fig. 6(c) can be explained using the effective model of a semi-infinite s/s+p-wave junction. We consider the pair potential on the s+p-wave side to be given by Eqs. (34) and (35), while, on the s-wave side, it has the form $\Delta_s s_y \tau_y$ with $\Delta_s = \Delta_0 e^{i\varphi}$. We assume that μ and t are the same on both sections of the junction. However, two sets of values are chosen such that one corresponds to the topological phase and the other to the trivial phase. We also take into account the strength of the interface barrier denoted by Z, but its value does not influence the key feature of our results. In order to calculate ABSs, we seek the solution of $M\hat{y} = 0$, where $\hat{y}$ is the envelope function composed of all the coefficients of the outgoing modes (see Appendix B). Then, the ABSs can be obtained from the condition $\det M = 0$. To make our plots clearer, we show $|\det M|^{\frac{1}{4}}$ as a function of energy E and phase difference φ. The dark blue curve indicates the ABSs in Figs. 7(a) and 7(c). In the topological phase, where the p-wave pairing is dominant, we can see that the energy of ABSs is described by $\pm\sin\varphi$ around the Fermi energy level, which is similar to the behavior observed above in the lattice model (see Fig. 6(c)). Thus, the Josephson current–phase relation is also approximated by nontrivial dependence $\sim \sin 2\varphi$, as shown in Fig. 7(b), apart from the standard 2π periodicity. Importantly, the observed double crossing points of ABSs around the Fermi energy, despite the fact that the nonzero interface barrier Z is explicitly introduced in the continuum model, confirm the topological origin of the obtained ABSs (MFs). As for the topologically trivial case in Fig. 7(c), where the s-wave component is dominant, the ABSs behave as $\sim \sqrt{1 - \sigma_N \sin^2\varphi/2}$. The corresponding current–phase relation has the standard $\sim \sin\varphi$ feature (see Fig. 7(d)). It is also seen that the ABSs are gapped around zero energy due to the presence of the interface barrier, which reveals its trivial nontopological nature.

We again emphasize here the importance of our result in this section: the ABS of the Josephson junction system that consists of DQWs has not been studied before. We investigate the ABS in this system and find the following. The ABS in the DQWs and conventional s-wave junction system shows $\sim \pm\sin\varphi$, which has not been observed in p-wave/p-wave or s-wave/s-wave Josephson junction systems. This curve is related to the presence of Kramers MFs by considering the coupling of Kramers MFs by second order. Further, this sinusoidal line is connected to the p-wave/s-wave junction system, which is justified by quasiclassical analysis.

5. Conclusion

In conclusion, we have systematically studied the pairing symmetry of the recently discovered topological double-quantum-wire (DQW) system. By taking into account the detuning of the chemical

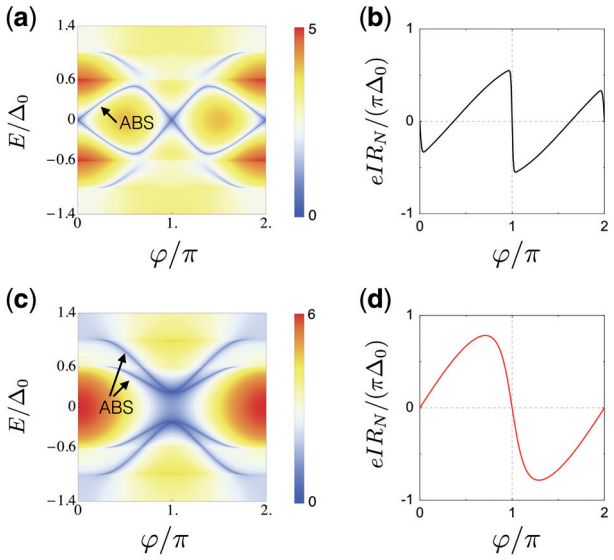

Fig. 7. The spectrum of ABSs (panels (a) and (c)) and Josephson current (panels (b) and (d)) in the s+p-wave/s-wave junction calculated in the continuum model. Panels (a) and (c) show $|\det M|^{\frac{1}{4}}$, where the dark blue curves indicate the positions of ABSs. Panels (b) and (d) show the current–phase relation normalized to the interface resistance R_N in the normal state. (a) and (b): $\Delta_0/\tilde{\mu} = 0.001$, $\Delta_s/\tilde{\mu} = 0.0004$, $k_F\Delta_p/\tilde{\mu} = 0.001$, and $\tilde{\mu} = 2t + \mu_s$. (c) and (d): $\Delta_0/\tilde{\mu} = 0.001$, $\Delta_s/\tilde{\mu} = 0.001$, and $k_F\Delta_p/\tilde{\mu} = 0.0004$. We use $Z = 0.5$ for all cases and set the temperature $k_BT = 0.01\Delta_0$ for panels (b) and (d). Notice that, when p-wave is dominant, the ABSs near the Fermi energy have the $\sim \sin\varphi$ feature, which corresponds to the nontrivial/trivial junction case shown in Fig. 6(c).

potential, we derive the generalized topological criterion for a DQW to host a Kramers pair of MFs as an ABS. We have also classified the symmetry of the superconducting order parameter by focusing on four degrees of freedom, i.e., frequency, spin, spatial parity inside the QWs, and spatial parity between the QWs. It is found that the magnitude of the odd-frequency pairing is hugely enhanced if topological superconductivity is achieved. It can be expected that the obtained odd-frequency pairings in the topological regime can be detected by tunneling spectroscopy [6,96–100] in experiments.

We have also investigated ABSs and the Josephson effect in DQW/DQW junctions. For topological/nontopological junctions, the energy dispersion of the ABSs is proportional to $\sim \pm\sin\varphi$, where φ denotes the phase difference between two sections of the DQW system. We have explained this behavior in terms of the couplings of Kramers pairs of MFs and spin-singlet s-wave Cooper pairs. We have confirmed that this φ dependence can be reproduced using the effective continuum model corresponding to the $s + p/s$-wave superconductor junction system. Our results can be explored for further experimental identification of the topological DQW system.

Acknowledgements

H.E. thanks P. Burset and K. T. Law for useful discussions. This work was supported by a Grant-in Aid for Scientific Research on Innovative Areas "Topological Material Science" (Grant No. 15H05853), a Grant-in-Aid for Scientific Research B (Grant No. 15H03686), a Grant-in-Aid for Challenging Exploratory Research (Grant No. 15K13498), and a Grant-in-Aid for JSPS Fellows (Grant No. 15J00565). We acknowledge support from the Swiss National Science Foundation and the NCCR QSIT.

Appendix A. Winding number

In this appendix, we introduce the winding number to help us to determine whether the zero-energy state described in the main text and shown in Fig. 2 is topologically protected. The procedure is as follows. First, we decompose the Hamiltonian into two sectors that are not coupled to each other. We note that the time-reversal partners always belong to different sectors. Second, we bring the chosen sector to the off-diagonal form and calculate its determinant. The winding number is given by considering how many times the vector composed of real and imaginary parts of the determinant wraps around the origin in the complex plane as a function of the momentum.

The model Hamiltonian given by Eq. (2) can be rewritten in the basis composed of $c'_{k_x} = (c_{k_x 1\uparrow}, c^\dagger_{-k_x 1\uparrow}, c_{k_x \bar{1}\uparrow}, c^\dagger_{-k_x \bar{1}\uparrow}, c_{k_x 1\downarrow}, c^\dagger_{-k_x 1\downarrow}, c_{k_x \bar{1}\downarrow}, c^\dagger_{-k_x \bar{1}\downarrow})^T$ as

$$\mathcal{H}(k_x) = \begin{pmatrix} A(k_x) & B(k_x) \\ -B(k_x) & A(k_x) \end{pmatrix}. \tag{A.1}$$

Here, $A(k_x)$ and $B(k_x)$ are 4×4 matrices given by

$$A(k_x) = \begin{pmatrix} \xi_{k_x 1} & 0 & 0 & 0 \\ 0 & -\xi_{k_x 1} & 0 & 0 \\ 0 & 0 & \xi_{k_x \bar{1}} & 0 \\ 0 & 0 & 0 & -\xi_{k_x \bar{1}} \end{pmatrix}, \tag{A.2}$$

$$B(k_x) = \begin{pmatrix} i2\alpha_1 \sin k_x a_x & \Delta_1 & 0 & \Delta_c \\ -\Delta_1 & -2i\alpha_1 \sin k_x a_x & -\Delta_c & 0 \\ 0 & \Delta_c & 2i\alpha_{\bar{1}} \sin k_x a_x & \Delta_{\bar{1}} \\ -\Delta_c & 0 & -\Delta_{\bar{1}} & -2i\alpha_{\bar{1}} \sin k_x a_x \end{pmatrix}. \tag{A.3}$$

In this basis, the time-reversal operator is represented as

$$\Theta = \begin{pmatrix} 0 & I_{4\times 4} \\ -I_{4\times 4} & 0 \end{pmatrix}. \tag{A.4}$$

We can easily confirm that $\Theta^\dagger \mathcal{H}(k_x)\Theta = \mathcal{H}^*(-k_x) = \mathcal{H}(k_x)$. Next, we transform the basis by unitary matrix V to satisfy

$$V^\dagger \Theta V = \begin{pmatrix} I_{4\times 4} & 0 \\ 0 & -I_{4\times 4} \end{pmatrix}, \tag{A.5}$$

where V can be written as

$$V = \frac{1}{\sqrt{2}} \begin{pmatrix} I_{4\times 4} & iI_{4\times 4} \\ iI_{4\times 4} & I_{4\times 4} \end{pmatrix}. \tag{A.6}$$

As a result, the Hamiltonian is given in the new basis by

$$V^\dagger \mathcal{H}(k_x) V = \begin{pmatrix} A(k_x) + iB(k_x) & 0 \\ 0 & A(k_x) - iB(k_x) \end{pmatrix} \equiv \begin{pmatrix} \mathcal{H}_1(k_x) & 0 \\ 0 & \mathcal{H}_2(k_x) \end{pmatrix} \tag{A.7}$$

and is decomposed into two independent sectors. In what follows, we focus on only one of the two sectors, $\mathcal{H}_1(k_x)$, given by

$$\mathcal{H}_1(k_x) = \begin{pmatrix} \xi_1 - 2\alpha_1 \sin k_x a_x & i\Delta_1 & 0 & i\Delta_c \\ -i\Delta_1 & -\xi_1 + 2\alpha_1 \sin k_x a_x & -i\Delta_c & 0 \\ 0 & i\Delta_c & \xi_{\bar{1}} - 2\alpha_{\bar{1}} \sin k_x a_x & i\Delta_1 \\ -i\Delta_c & 0 & -i\Delta_1 & -\xi_{\bar{1}} + 2\alpha_{\bar{1}} \sin k_x a_x \end{pmatrix}. \tag{A.8}$$

$\mathcal{H}_1(k_x)$ possesses chiral symmetry, $C\mathcal{H}_1(k_x)C = -\mathcal{H}_1(k_x)$, where

$$C = \begin{pmatrix} 0 & 1 & 0 & 0 \\ 1 & 0 & 0 & 0 \\ 0 & 0 & 0 & 1 \\ 0 & 0 & 1 & 0 \end{pmatrix}. \tag{A.9}$$

We also define W as

$$W = \begin{pmatrix} 1 & 0 & 1 & 0 \\ 1 & 0 & -1 & 0 \\ 0 & 1 & 0 & 1 \\ 0 & 1 & 0 & -1 \end{pmatrix} \tag{A.10}$$

such that

$$W^\dagger C W = \begin{pmatrix} I_{2\times 2} & 0 \\ 0 & -I_{2\times 2} \end{pmatrix}. \tag{A.11}$$

Using the matrix W, $\mathcal{H}_1(k_x)$ is transformed into

$$\mathcal{H}_1'(k_x) = W^\dagger \mathcal{H}_1(k_x) W = \begin{pmatrix} 0 & h_1(k_x) \\ h_1^\dagger(k_x) & 0 \end{pmatrix}, \tag{A.12}$$

where

$$h_1(k_x) = \begin{pmatrix} \xi_{k_x 1} - 2\alpha_1 \sin k_x a_x - i\Delta_1 & -i\Delta_c \\ -i\Delta_c & \xi_{k_x \bar{1}} - 2\alpha_{\bar{1}} \sin k_x a_x - i\Delta_1 \end{pmatrix}. \tag{A.13}$$

This allows us to easily calculate the determinant D as

$$D_1 = \det[h_1(k_x)] = (\xi_{k_x 1} - 2\alpha_1 \sin k_x a_x - i\Delta_1) \times (\xi_{k_x \bar{1}} - 2\alpha_{\bar{1}} \sin k_x a_x - i\Delta_1) + \Delta_c^2. \tag{A.14}$$

The winding number is given by [101]

$$\nu_1 = \frac{1}{2\pi i} \oint (D_1^{-1} dD_1). \tag{A.15}$$

The integer ν_1 corresponds to the number of times that the vector composed of the real and imaginary parts of D wraps around the origin in the complex plane when we change the momentum from $k_x a_x =$

$-\pi$ to $k_x a_x = \pi$. To simplify calculations, it is useful to introduce symmetric and antisymmetric parameters:

$$\alpha_{s/a} = (\alpha_1 \pm \alpha_{\bar{1}})/2,$$
$$\mu_{s/a} = (\mu_1 \pm \mu_{\bar{1}})/2. \tag{A.16}$$

The real and imaginary parts of $\det[h_1(k_x)]$ are rewritten as

$$\begin{aligned}\lambda(k_x) &\equiv \mathrm{Re}\big[\det[h_1(k_x)]\big] = -(\mu_a + 2\alpha_a \sin k_x a_x)^2 + \Delta_c^2 \\ &\quad - \Delta_1^2 + (2t\cos k_x a_x + \mu_s + 2\alpha_s \sin k_x a_x)^2, \qquad \text{(A.17)} \\ \varepsilon(k_x) &\equiv \mathrm{Im}\big[\det[h_1(k_x)]\big] \\ &= 2\Delta_1(2t\cos k_x a_x + 2\alpha_s \sin k_x a_x + \mu_s). \qquad \text{(A.18)}\end{aligned}$$

Here, we assume $\sqrt{4t^2 + 4\alpha_s^2} < |\mu_s|$ such that $\varepsilon(k_x)$ becomes zero at certain values of k_x. Based on the spirit of the "weak pairing limit" [61,102], we discuss the winding number [101]. The winding number is equivalent to the wrapping number of the normalized vector

$$(d_1, d_2) \equiv \left(\frac{\lambda(k_x)}{\sqrt{\varepsilon^2(k_x) + \lambda^2(k_x)}}, \frac{\varepsilon(k_x)}{\sqrt{\varepsilon^2(k_x) + \lambda^2(k_x)}}\right) \tag{A.19}$$

around the origin in complex space as k_x changes from $k_x a_x = -\pi$ to $k_x a_x = \pi$. We scale $\lambda(k_x)$ to $\lambda(k_x) \to a\lambda(k_x)$ by introducing a parameter a, and continuously change a from $a = 1$ to a small nonzero value. Importantly, upon this change, the winding number remains the same. In the case of $\varepsilon(k_x) \neq 0$, (d_1, d_2) is approximated as $(0, \mathrm{sgn}\ \varepsilon(k_x)) \equiv (0, \pm 1)$ for a sufficiently small a and stays constant. However, in the vicinity of Fermi momenta $k_{F,j}$, which we define as two solutions of $\varepsilon(k_{F,j}) = 0$ such that $k_{F,1} < k_{F,2}$, the (d_1, d_2) vector could wind around the origin. Close to these momenta, $\varepsilon(k_x)$ can be expanded as

$$\varepsilon(k_x) = [\partial_{k_x}\varepsilon](k_x - k_{F,j}) + \cdots. \tag{A.20}$$

Around the momentum $k_{F,j}$, the vector (d_1, d_2) reads

$$\begin{aligned} d_1 &= \frac{a\lambda(k_x)}{\sqrt{(\partial_{k_x}\varepsilon)^2(k_x - k_{F,j})^2 + a^2\lambda^2(k_x)}}, \\ d_2 &= \frac{[\partial_{k_x}\varepsilon][(k_x - k_{F,j})]}{\sqrt{(\partial_{k_x}\varepsilon)^2(k_x - k_{F,j})^2 + a^2\lambda^2(k_x)}}. \end{aligned} \tag{A.21}$$

Now we consider the trajectory spanned the the vector (d_1, d_2) as the momentum changes from $k_x a_x = -\pi$ to $k_x a_x = \pi$; see also Fig. A1(a). As we have explained above, only parts of the trajectory close to $k_x = k_{F,1}$ and $k_x = k_{F,2}$ contribute to the winding number. Thus, we only focus on the trajectory around these momenta. If we consider k_x changing as

$$\begin{aligned}(k_x < k_{F,1}) &\to (k_x = k_{F,1}) \to (k_{F,1} < k_x < k_{F,2}) \\ &\to (k_x = k_{F,2}) \to (k_x > k_{F,2}),\end{aligned}$$

the vector (d_1, d_2) changes accordingly as

$$\begin{aligned}(0, \mathrm{sgn}[\varepsilon(k_x < k_{F,1})]) &\to (\mathrm{sgn}[\lambda(k_{F,1})], 0) \to (0, \mathrm{sgn}[\varepsilon]) \\ &\to (\mathrm{sgn}[\lambda(k_{F,2})], 0) \to (0, \mathrm{sgn}[\varepsilon(k_x > k_{F,2})]).\end{aligned}$$

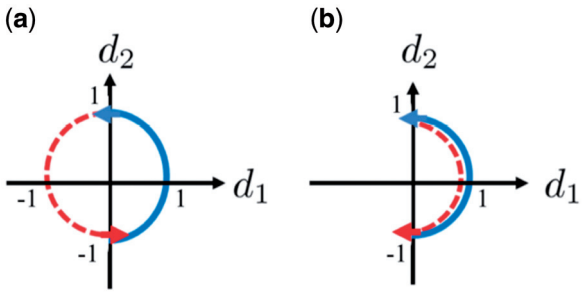

Fig. A1. (a) The trajectory, spanned by the vector (d_1, d_2) in the case of $\mathrm{sgn}[\lambda(k_{F,1})] = -\mathrm{sgn}[\lambda(k_{F,2})]$, wraps around the origin leading to the topologically nontrivial state. (b) The trajectory, spanned by the vector (d_1, d_2) in the case of $\mathrm{sgn}[\lambda(k_{F,1})] = \mathrm{sgn}[\lambda(k_{F,2})]$, does not go around the origin, demonstrating that the system is topologically trivial.

If $\mathrm{sgn}[\lambda(k_{F,1})] = -\mathrm{sgn}[\lambda(k_{F,2})]$, the trajectory of the vector (d_1, d_2) wraps around the origin (see Fig. A1(b)), indicating a topologically nontrivial state. On the other hand, if $\mathrm{sgn}[\lambda(k_{F,1})] = \mathrm{sgn}[\lambda(k_{F,2})]$, the trajectory does not wind around the origin (see Fig. A1(b)) and the system is in the trivial state. Therefore, we can define the topological condition as follows:

$$(-1)^{\nu} = \prod_{k_x = k_{F,1}, k_{F,2}} \mathrm{sgn}[\Delta_c^2 - \Delta_1^2 - (\mu_a + 2\alpha_a \sin k_x a_x)^2], \tag{A.22}$$

where for $\nu = 1(0)$ the system is in a nontrivial (trivial) topological state.

Appendix B. Quasiclassical analysis of the effective model

In this appendix we use the effective Hamiltonian given by Eq. (33) to calculate the ABS spectrum and Josephson current in DQW/DQW junctions. Also, we focus on the most interesting scenario where the left DQW is in the topologically nontrivial phase while the right DQW is in the trivial phase. The system can be viewed as an s+p/s-wave junction. Since time-reversal symmetry is respected, the Josephson current has the property $I(\varphi) = -I(-\varphi)$. The s+p/s-wave junction with $\Delta_{s+p} = |\Delta_{s+p}| e^{i\varphi}$ and $\Delta_s = |\Delta_s|$ is equivalent to the s/s+p-wave junction with $\Delta_s = |\Delta_s| e^{i\varphi}$ and $\Delta_{s+p} = |\Delta_{s+p}|$. In the following calculation, we adopt the latter convention, such that Furusaki–Tsukada's formula [103] can be applied directly. We consider a semi-infinite junction wherein an insulating barrier at $x = 0$ separates an s-wave superconductor and an s+p-wave superconductor. The Hamiltonian of this system is given by

$$H = H_s + H_I + H_{s+p}, \tag{B.1}$$

$$H_s = \left(k_x^2/2m - \mu_0\right) \tau_z - \Delta_0 e^{i\varphi} s_y \tau_y, \tag{B.2}$$

$$H_I = H_\delta \delta(x) \tau_z, \tag{B.3}$$

$$H_{s+p} = \left(k_x^2/2m - \tilde{\mu}\right) \tau_z - \left(\Delta_s + k_x s_y \Delta_p\right) s_y \tau_y, \tag{B.4}$$

where φ describes a macroscopic phase difference between the two sections and $\tilde{\mu} = \mu_s + 2t$. For simplicity, we assume that the chemical potential is the same in all regions, $\mu_0 = \tilde{\mu}$, and the interface barrier is modeled by a δ function with a strength H_δ. Taking into account the Andreev approximation, we can write down the eigenmodes of the Hamiltonians H_s and H_{s+p}. In the s-wave-superconductor-dominated section ($x < 0$), we find

$$\psi_{\uparrow,\pm}^{s,e}(x) = \left[e^{i\varphi/2}, 0, 0, \gamma_0 e^{-i\varphi/2}\right]^T e^{\pm i k_F x}, \tag{B.5a}$$

$$\psi^{s,e}_{\downarrow,\pm}(x) = \left[0, e^{i\varphi/2}, -\gamma_0 e^{-i\varphi/2}, 0\right]^T e^{\pm ik_F x}, \tag{B.5b}$$

$$\psi^{s,h}_{\uparrow,\pm}(x) = \left[\gamma_0 e^{i\varphi/2}, 0, 0, e^{-i\varphi/2}\right]^T e^{\mp ik_F x}, \tag{B.5c}$$

$$\psi^{s,h}_{\downarrow,\pm}(x) = \left[0, \gamma_0 e^{i\varphi/2}, -e^{-i\varphi/2}, 0\right]^T e^{\mp ik_F x}, \tag{B.5d}$$

where we have defined $k_F = \sqrt{2m\tilde{\mu}}$ and $\gamma_0 = \Delta_0(E + \sqrt{E^2 - \Delta_0^2})^{-1}$. The quasiparticle energy E is measured from the chemical potential and the subscript "+" ("−") stands for the right-going (left-going) solutions. For the s+p-wave-superconductor-dominated section ($x > 0$), we only consider the right-going solutions of H_{s+p} given by

$$\psi^{s+p,e}_1(x) = [1, -i, i\gamma_1, \gamma_1]^T e^{ik_F x}, \tag{B.6a}$$

$$\psi^{s+p,e}_2(x) = [1, i, -i\gamma_2, \gamma_2]^T e^{ik_F x}, \tag{B.6b}$$

$$\psi^{s+p,h}_1(x) = [\gamma_1, i\gamma_1, -i, 1]^T e^{-ik_F x}, \tag{B.6c}$$

$$\psi^{s+p,h}_2(x) = [\gamma_2, -i\gamma_2, i, 1]^T e^{-ik_F x}, \tag{B.6d}$$

with $\gamma_{1(2)} = \left(\Delta_s \mp k_F\Delta_p\right)[E + \sqrt{E^2 - \left(\Delta_s \mp k_F\Delta_p\right)^2}]^{-1}$ reflecting the existence of two superconducting gaps $\Delta_1 = \left|\Delta_s - k_F\Delta_p\right|$ and $\Delta_2 = \left|\Delta_s + k_F\Delta_p\right|$. In order to obtain the ABSs, we consider the following wave function:

$$\Psi_s(x) = \sum_{\sigma=\uparrow,\downarrow} r^{s,e}_\sigma \psi^{s,e}_{\sigma,-}(x) + r^{s,h}_\sigma \psi^{s,h}_{\sigma,-}(x), \quad x < 0 \tag{B.7}$$

$$\Psi_{s+p}(x) = \sum_{\nu=1,2} r^{s+p,e}_\nu \psi^{s+p,e}_\nu(x) + r^{s+p,h}_\nu \psi^{s+p,h}_\nu(x), \quad x > 0. \tag{B.8}$$

The scattering coefficients $r^{s,e}_\sigma$, $r^{s,h}_\sigma$, $r^{s+p,e}_\nu$, and $r^{s+p,h}_\nu$ are chosen such that the boundary conditions at $x = 0$ are satisfied:

$$\Psi_s(0) = \Psi_{s+p}(0), \tag{B.9}$$

$$\partial_x\Psi_{s+p}(0) - \partial_x\Psi_s(0) = 2mH_\delta\Psi_s(0). \tag{B.10}$$

The discrete ABSs can be determined by the condition $\det M = 0$, where the matrix M is defined as

$$M = \begin{bmatrix} M_1 & M_2 \\ M_3 & M_4 \end{bmatrix}, \tag{B.11}$$

$$M_1 = \begin{bmatrix} 0 & \gamma_0 e^{i\varphi/2} & 0 & e^{i\varphi/2} \\ \gamma_0 e^{i\varphi/2} & 0 & e^{i\varphi/2} & 0 \\ -e^{-i\varphi/2} & 0 & -\gamma_0 e^{-i\varphi/2} & 0 \\ 0 & e^{-i\varphi/2} & 0 & \gamma_0 e^{-i\varphi/2} \end{bmatrix}, \tag{B.12}$$

$$M_2 = \begin{bmatrix} -1 & -\gamma_1 & -1 & -\gamma_2 \\ i & -i\gamma_1 & -i & i\gamma_2 \\ -i\gamma_1 & i & i\gamma_2 & -i \\ -\gamma_1 & -1 & -\gamma_2 & -1 \end{bmatrix}, \tag{B.13}$$

$$M_3 = \begin{bmatrix} 0 & (1-iZ)\gamma_0 e^{i\varphi/2} & 0 & (-1-iZ)e^{i\varphi/2} \\ (1-iZ)\gamma_0 e^{i\varphi/2} & 0 & (-1-iZ)e^{i\varphi/2} & 0 \\ -(1-iZ)e^{-i\varphi/2} & 0 & (1+iZ)\gamma_0 e^{-i\varphi/2} & 0 \\ 0 & (1-iZ)e^{-i\varphi/2} & 0 & (-1-iZ)\gamma_0 e^{-i\varphi/2} \end{bmatrix}, \tag{B.14}$$

$$M_4 = \begin{bmatrix} -1 & \gamma_1 & -1 & \gamma_2 \\ i & i\gamma_1 & -i & -i\gamma_2 \\ -i\gamma_1 & -i & i\gamma_2 & i \\ -\gamma_1 & 1 & -\gamma_2 & 1 \end{bmatrix}, \tag{B.15}$$

where we have used the notation $Z = 2mH_\delta/k_F$.

At the next step, we calculate the Josephson current using Furusaki–Tsukada's formula [103] by considering the incoming electrons from the left side:

$$\Psi^{s,e}_{\uparrow}(x) = \psi^{s,e}_{\uparrow,+}(x) + \sum\nolimits_{\sigma}\left[r^{ee}_{\uparrow\sigma}\psi^{s,e}_{\sigma,-}(x) + r^{eh}_{\uparrow\sigma}\psi^{s,h}_{\sigma,-}(x)\right], \tag{B.16a}$$

$$\Psi^{s,e}_{\downarrow}(x) = \psi^{s,e}_{\downarrow,+}(x) + \sum\nolimits_{\sigma}\left[r^{ee}_{\downarrow\sigma}\psi^{s,e}_{\sigma,-}(x) + r^{eh}_{\downarrow\sigma}\psi^{s,h}_{\sigma,-}(x)\right], \tag{B.16b}$$

$$\Psi^{s,h}_{\uparrow}(x) = \psi^{s,h}_{\uparrow,+}(x) + \sum\nolimits_{\sigma}\left[r^{he}_{\uparrow\sigma}\psi^{s,e}_{\sigma,-}(x) + r^{hh}_{\uparrow\sigma}\psi^{s,h}_{\sigma,-}(x)\right], \tag{B.16c}$$

$$\Psi^{s,h}_{\downarrow}(x) = \psi^{s,h}_{\downarrow,+}(x) + \sum\nolimits_{\sigma}\left[r^{he}_{\downarrow\sigma}\psi^{s,e}_{\sigma,-}(x) + r^{hh}_{\downarrow\sigma}\psi^{s,h}_{\sigma,-}(x)\right]. \tag{B.16d}$$

All the coefficients can be found from the same boundary conditions given by Eq. (B.10). The Josephson current is given by [103]

$$I = \frac{e\Delta_0}{2}k_B T \sum_{\omega_n,\sigma}\frac{\mathrm{sgn}(\omega_n)}{\Omega_n}\left[r^{eh}_{\sigma\sigma}(i\omega_n) - r^{he}_{\sigma\sigma}(i\omega_n)\right], \tag{B.17}$$

where $r^{eh}_{\sigma\sigma}(i\omega_n)$ and $r^{he}_{\sigma\sigma}(i\omega_n)$ are obtained by the analytical continuation $E \to i\omega_n$ of $r^{eh}_{\sigma\sigma}(E)$ and $r^{he}_{\sigma\sigma}(E)$. The Matsubara frequency ω_n is defined as $\omega_n = \pi k_B T(2n+1)$ for $n = 0, \pm1, \pm2, \ldots$, and $\Omega_n = \sqrt{\omega_n^2 + \Delta_0^2}$. Here, we work in the low-temperature limit and neglect the temperature dependence of the superconducting gap.

References

[1] A. P. Schnyder, S. Ryu, A. Furusaki, and A. W. W. Ludwig, Phys. Rev. B **78**, 195125 (2008).
[2] A. Kitaev, AIP Conf. Proc. **1134**, 22 (2009).
[3] L. J. Buchholtz and G. Zwicknagl, Phys. Rev. B **23**, 5788 (1981).
[4] J. Hara and K. Nagai, Prog. Theor. Phys. **76**, 1237 (1986).
[5] C. R. Hu, Phys. Rev. Lett. **72**, 1526 (1994).
[6] Y. Tanaka and S. Kashiwaya, Phys. Rev. Lett. **74**, 3451 (1995).
[7] S. Kashiwaya and Y. Tanaka, Rep. Prog. Phys. **63**, 1641 (2000).
[8] M. Sato, Y. Tanaka, K. Yada, and T. Yokoyama, Phys. Rev. B **83**, 224511 (2011).
[9] Y. Tanaka, M. Sato, and N. Nagaosa, J. Phys. Soc. Jpn. **81**, 011013 (2012).
[10] S. Kobayashi, K. Shiozaki, Y. Tanaka, and M. Sato, Phys. Rev. B **90**, 024516 (2014).
[11] S. Kobayashi, Y. Tanaka, and M. Sato, arXiv:1510.01411 [cond-mat.supr-con] [Search INSPIRE].
[12] M. Sato and S. Fujimoto, Phys. Rev. B **79**, 094504 (2009).
[13] R. M. Lutchyn, J. D. Sau, and S. Das Sarma, Phys. Rev. Lett. **105**, 077001 (2010).
[14] Y. Oreg, G. Refael, and F. von Oppen, Phys. Rev. Lett. **105**, 177002 (2010).
[15] J. Alicea, Phys. Rev. B **81**, 125318 (2010).
[16] D. Chevallier, P. S. D. Sticlet, and C. Bena, Phys. Rev. B **85**, 23530 (2012).
[17] J. Klinovaja, S. Gangadharaiah, and D. Loss, Phys. Rev. Lett. **108**, 196804 (2012).

[18] J. Alicea, Rep. Prog. Phys. **75**, 076501 (2012).
[19] J. Klinovaja, G. J. Ferreira, and D. Loss, Phys. Rev. B **86**, 235416 (2012).
[20] C. W. J. Beenakker, Annu. Rev. Condens. Matter Phys. **4**, 113 (2013).
[21] J. Klinovaja, P. Stano, A. Yazdani, and D. Loss, Phys. Rev. Lett. **111**, 186805 (2013).
[22] S. Nadj-Perge, I. K. Drozdov, B. A. Bernevig, and A. Yazdani, Phys. Rev. B **88**, 020407 (2013).
[23] J. Klinovaja and D. Loss, Phys. Rev. Lett. **112**, 246403 (2014).
[24] H. Ebisu, B. Lu, K. Taguchi, A. A. Golubov, and Y. Tanaka, Phys. Rev. B **93**, 024509 (2016).
[25] V. Mourik, K. Zuo, S. Frolov, E. P. A. M. Bakkers, S. Plissard, and L. P. Kouwenhoven, Science **336**, 1003 (2012).
[26] M. Deng, C. Yu, G. Huang, M. Larsson, P. Caroff, and H. Xu, Nano Lett. **12**, 6414 (2012).
[27] L. Rokhinson, X. Liu, and J. Furdyna, Nat. Phys. **8**, 795 (2012).
[28] A. Das, Y. Ronen, Y. Most, Y. Oreg, and M. H. H. Shtrikman, Nat. Phys. **8**, 887 (2012).
[29] S. Nadj-Perge, I. K. Drozdov, J. Li, H. Chen, S. Jeon, J. Seo, A. H. MacDonald, B. A. Bernevig, and A. Yazdani, Science **346**, 602 (2014).
[30] R. Pawlak, M. Kisiel, J. Klinovaja, T. Meier, S. Kawai, T. Glatzel, D. Loss, and E. Meyer, arXiv:1505.06078 [physics.atm-clus] [Search INSPIRE].
[31] C. Nayak, S. H. Simon, A. Stern, M. Freedman, and S. Das Sarma, Rev. Mod. Phys. **80**, 1083 (2008).
[32] J. Alicea, Y. Oreg, G. Refael, F. von Oppen, and M. Fisher, Nat. Phys. **7**, 412 (2011).
[33] V. L. Berezinskii, JETP Lett. **20**, 287 (1974).
[34] A. Balatsky and E. Abrahams, Phys. Rev. B **45**, 13125 (1992).
[35] P. Coleman, A. Georges, and A. M. Tsvelik, J. Phys.: Condens. Matter **9**, 345 (1997).
[36] Y. Fuseya, H. Kohno, and K. Miyake, J. Phys. Soc. Jpn. **72**, 2914 (2003).
[37] Y. Tanaka, A. A. Golubov, S. Kashiwaya, and M. Ueda, Phys. Rev. Lett. **99**, 037005 (2007).
[38] Y. Tanaka and A. A. Golubov, Phys. Rev. Lett. **98**, 037003 (2007).
[39] Y. Tanaka, Y. Tanuma, and A. A. Golubov, Phys. Rev. B **76**, 054522 (2007).
[40] M. Eschrig, T. Löfwander, T. Champel, J. Cuevas, and G. Schön, J. Low Temp. Phys. **147**, 457 (2007).
[41] Y. Asano and Y. Tanaka, Phys. Rev. B **87**, 104513 (2013).
[42] R. Wakatsuki, M. Ezawa, Y. Tanaka, and N. Nagaosa, Phys. Rev. B **90**, 014505 (2014).
[43] H. Ebisu, K. Yada, H. Kasai, and Y. Tanaka, Phys. Rev. B **91**, 054518 (2015).
[44] L. Fu and C. L. Kane, Phys. Rev. Lett. **100**, 096407 (2008).
[45] K. Sun, C.-K. Chiu, H.-H. Hung, and J. Wu, Phys. Rev. B **89**, 104519 (2014).
[46] J. Klinovaja and D. Loss, Phys. Rev. B **92**, 121410 (2015).
[47] C. Schrade, A. A. Zyuzin, J. Klinovaja, and D. Loss, arXiv:1506.09120 [cond-mat.mes-hall] [Search INSPIRE].
[48] L. Fu and C. L. Kane, Phys. Rev. Lett. **102**, 216403 (2009).
[49] S. Nakosai, Y. Tanaka, and N. Nagaosa, Phys. Rev. Lett. **108**, 147003 (2012).
[50] C. L. M. Wong and K. T. Law, Phys. Rev. B **86**, 184516 (2012).
[51] S. Nakosai, J. C. Budich, Y. Tanaka, B. Trauzettel, and N. Nagaosa, Phys. Rev. Lett. **110**, 117002 (2013).
[52] A. Keselman, L. Fu, A. Stern, and E. Berg, Phys. Rev. Lett. **111**, 116402 (2013).
[53] E. Gaidamauskas, J. Paaske, and K. Flensberg, Phys. Rev. Lett. **112**, 126402 (2014).
[54] A. Haim, A. Keselman, E. Berg, and Y. Oreg, Phys. Rev. B **89**, 220504 (2014).
[55] J. Klinovaja, P. Stano, and D. Loss, arXiv:1510.03640 [cond-mat.mes-hall] [Search INSPIRE].
[56] F. Zhang, C. L. Kane, and E. J. Mele, Phys. Rev. Lett. **111**, 056402 (2013).
[57] S. Deng, L. Viola, and G. Ortiz, Phys. Rev. Lett. **108**, 036803 (2012).
[58] J. Klinovaja, A. Yacoby, and D. Loss, Phys. Rev. B **90**, 155447 (2014).
[59] S. B. Chung, J. Horowitz, and X.-L. Qi, Phys. Rev. B **88**, 214514 (2013).
[60] X.-L. Qi, T. L. Hughes, S. Raghu, and S.-C. Zhang, Phys. Rev. Lett. **102**, 187001 (2009).
[61] X.-L. Qi, T. L. Hughes, and S.-C. Zhang, Phys. Rev. B **81**, 134508 (2010).
[62] J. Klinovaja and D. Loss, Phys. Rev. B **90**, 045118 (2014).
[63] P. Recher, E. V. Sukhorukov, and D. Loss, Phys. Rev. B **63**, 165314 (2001).
[64] B. Braunecker, P. Burset, and A. Levy Yeyati, Phys. Rev. Lett. **111**, 136806 (2013).
[65] G. Deutscher and D. Feinberg, Appl. Phys. Lett. **76**, 487 (2000).
[66] D. Beckmann, H. B. Weber, and H. v. Löhneysen, Phys. Rev. Lett. **93**, 197003 (2004).
[67] S. Russo, M. Kroug, T. M. Klapwijk, and A. F. Morpurgo, Phys. Rev. Lett. **95**, 027002 (2005).
[68] L. Hofstetter, J. Nygard, and C. Schonenberger, Nature **461**, 960 (2009).

[69] L. G. Herrmann, F. Portier, P. Roche, A. L. Yeyati, T. Kontos, and C. Strunk, Phys. Rev. Lett. **104**, 026801 (2010).
[70] P. Burset, W. J. Herrera, and A. L. Yeyati, Phys. Rev. B **84**, 115448 (2011).
[71] K. Sato, D. Loss, and Y. Tserkovnyak, Phys. Rev. B **85**, 235433 (2012).
[72] J. Klinovaja and D. Loss, Phys. Rev. B **86**, 085408 (2012).
[73] D. Rainis, L. Trifunovic, J. Klinovaja, and D. Loss, Phys. Rev. B **87**, 024515 (2013).
[74] B. Braunecker, G. I. Japaridze, J. Klinovaja, and D. Loss, Phys. Rev. B **82**, 045127 (2010).
[75] F. S. Bergeret, A. F. Volkov, and K. B. Efetov, Phys. Rev. Lett. **86**, 4096 (2001).
[76] F. S. Bergeret, A. F. Volkov, and K. B. Efetov, Rev. Mod. Phys. **77**, 1321 (2005).
[77] M. Eschrig, J. Kopu, J. C. Cuevas, and G. Schön, Phys. Rev. Lett. **90**, 137003 (2003).
[78] M. Eschrig, Rep. Prog. Phys. **78**, 104501 (2015).
[79] A. M. Black-Schaffer and A. V. Balatsky, Phys. Rev. B **88**, 104514 (2013).
[80] F. Parhizgar and A. M. Black-Schaffer, Phys. Rev. B **90**, 184517 (2014).
[81] L. Komendová, A. V. Balatsky, and A. M. Black-Schaffer, Phys. Rev. B **92**, 094517 (2015).
[82] Y. Asano and A. Sasaki, Phys. Rev. B **92**, 224508 (2015).
[83] S. Hoshino, Phys. Rev. B **90**, 115154 (2014).
[84] K. Yada, S. Onari, and Y. Tanaka, Physica C **469**, 991 (2009).
[85] T. Yokoyama, Y. Tanaka, and A. A. Golubov, Phys. Rev. B **78**, 012508 (2008).
[86] A. Furusaki and M. Tsukada, Phys. Rev. B **43**, 10164 (1991).
[87] H.-J. Kwon, K. Sengupta, and V. Yakovenko, Eur. Phys. J. B **37**, 349 (2004).
[88] A. Y. Kitaev, Usp. Fiz. Nauk (Suppl.) **171**, 131 (2001).
[89] Y. Tanaka and S. Kashiwaya, Phys. Rev. B **56**, 892 (1997).
[90] T. Ojanen, Phys. Rev. B **87**, 100506 (2013).
[91] C. Spånslätt, E. Ardonne, J. C. Budich, and T. H. Hansson, J. Phys.: Condens. Matter **27**, 405701 (2015).
[92] J. Klinovaja and D. Loss, Eur. Phys. J. B **88**, 62 (2015).
[93] X.-J. Liu, C. L. M. Wong, and K. T. Law, Phys. Rev. X **4**, 021018 (2014).
[94] L. Klam, A. Epp, W. Chen, M. Sigrist, and D. Manske, Phys. Rev. B **89**, 174505 (2014).
[95] Y. Tanaka, T. Yokoyama, A. V. Balatsky, and N. Nagaosa, Phys. Rev. B **79**, 060505 (2009).
[96] K. T. Law, P. A. Lee, and T. K. Ng, Phys. Rev. Lett. **103**, 237001 (2009).
[97] H. Kwon, K. Sengupta, and V. Yakovenko, Eur. Phys. J. B **37**, 349 (2004).
[98] C. J. Bolech and E. Demler, Phys. Rev. Lett. **98**, 237002 (2007).
[99] Y. Tanaka, T. Yokoyama, and N. Nagaosa, Phys. Rev. Lett. **103**, 107002 (2009).
[100] J. Linder, Y. Tanaka, T. Yokoyama, A. Sudbo, and N. Nagaosa, Phys. Rev. Lett. **104**, 067001 (2010).
[101] X. G. Wen and A. Zee, Nucl. Phys. B **316**, 641 (1989).
[102] M. Sato, Phys. Rev. B **81**, 220504 (2010).
[103] A. Furusaki and M. Tsukada, Solid State Commun. **299**, 78 (1991).